Stability Analysis of a PMSG-Based Large Offshore Wind Farm Connected to a VSC-HVDC

Linash P. Kunjumuhammed, *Senior Member, IEEE*, Bikash C. Pal, *Fellow, IEEE*, Robin Gupta, and Kevin J. Dyke, *Senior Member, IEEE*

***Abstract*—This paper presents modal analysis of a large offshore wind farm using permanent magnet synchronous generator (PMSG)-type wind turbines connected to a voltage source converter HVDC (VSC-HVDC). Multiple resonant frequencies are observed in the ac grid of offshore wind farms. Their control is crucial for the uninterrupted operation of the wind farm system. The characteristics of oscillatory modes are presented using modal analysis and participation factor analysis. Sensitivity of critical modes to wind turbine design parameters and their impact on closed loop stability of the system are discussed. A comparison between a full wind farm model and an aggregated model is presented to show differences in the characteristics of critical modes observed in the models, and implication of using the models for stability studies It is concluded that robust control design is important for reliable operation of the system.**

I. Introduction

MANY countries are developing offshore wind farms of several hundred MW capacity in order to meet their future energy demand. These wind farms are being located far away from the shore which makes HVDC transmission using voltage source converter (VSC) a preferred option. The North Sea has 68 GW wind potential to be harnessed by six countries [1]. So meshed HVDC is a suitable choice. The offshore ac system in such cases is a local synchronous system connecting hundreds of wind turbine generators (WTGs) and the VSC intake point.

The wind farm systems are reported to contain multiple resonance modes in the collector network [2] that can cause operational issues. The number of modes and their characteristics can vary as the operating configurations changes for several reasons such as: prevailing wind speed, wind direction, wake effect, availability of individual WTGs for maintenance, and the energy requirements from the main grid. The impedance of the system and the number of WTGs present at an instant determine the characteristics of electrical oscillatory modes.

A detailed harmonic analysis of the wind farm system can provide insight about the electrical oscillatory modes [3]. This requires detailed harmonic model and relevant data from the WTG and VSC manufacturer. However, the harmonic characteristics of the devices may not remain constant and can vary with operating conditions [3], [4]. Some of the recent works reported on the interaction of wind turbines and HVDC converters use aggregate modelling of wind farms [5]–[9]. The aggregation can reduce computation time but may misrepresent some of the important characteristics of the wind farm modes.

In this paper, a modal analysis of the wind farm using detailed representation of its components is carried out to understand the nature of dynamic interaction. The model is useful to investigate the characteristics of different oscillatory modes present in the wind farm system. A sensitivity analysis is conducted to assess stability of the wind farm system to changes in WTG design parameters, which is not possible using traditional harmonic method.

A 630 MW wind farm system model using permanent magnet synchronous generator (PMSG) type WTGs having close resemblance to practical wind farm system is considered in this paper. The details of the wind farm and modelling aspects of different wind farm components are discussed in Section II and Section III, respectively. Sensitivity studies for critical modes against WTG design parameters such as Grid Side Converter (GSC) controller, Phase Locked Loop (PLL) and filter are conducted for deeper understanding and control solution of the resonance problem. Section IV presents different designs for GSC controller, PLLs and the filter that are used for the modal analysis and sensitivity analysis. Section V presents modal analysis of a single machine infinite bus (SMIB) test system, and establishes characteristics of various oscillatory modes. In the wind farm many WTGs are accumulated to form a string, many strings forms an area, and four areas form the wind farm system. The Section VI discusses the evolution of modes as the complexity of system changes. Four critical modes are selected from the wind farm system for detailed analysis that is presented in the Section VII. Section VIII discusses design of a VSC controller for the wind farm system and shows how different WTG designs affect closed loop stability of the wind farm using eigenvalue analysis and dynamic simulation. Differences between characteristics of oscillatory modes obtained from a full wind farm system and an aggregated model is presented in Section IX.

Manuscript received August 19, 2016; revised November 22, 2016 and March 7, 2017; accepted May 12, 2017. Date of publication June 26, 2017; date of current version August 18, 2017. This work was supported in part by EPSRC U.K., under Grant Stability and Control of Power Networks with Energy Storage (STABLE-NET) U.K.-China Grid Scale Storage (EP/L014343/1) and in part by GE's Grid Solutions. Paper no. TEC-00714-2016. *(Corresponding author: Bikash Chandra Pal.)*

L. P. Kunjumuhammed and B. C. Pal are with the Electrical and Electronic Engineering Department, Imperial College, London SW7 2AZ U.K. (e-mail: linash.p.k@imperial.ac.uk; b.pal@imperial.ac.uk).

R. Gupta and K. J. Dyke are with the GE's Grid Solutions, Stafford SW7-2BT U.K. (e-mail: robin.gupta@alstom.com; kevin.dyke@alstom.com)

Color versions of one or more of the figures in this paper are available online at http://ieeexplore.ieee.org.

Digital Object Identifier 10.1109/TEC.2017.2705801

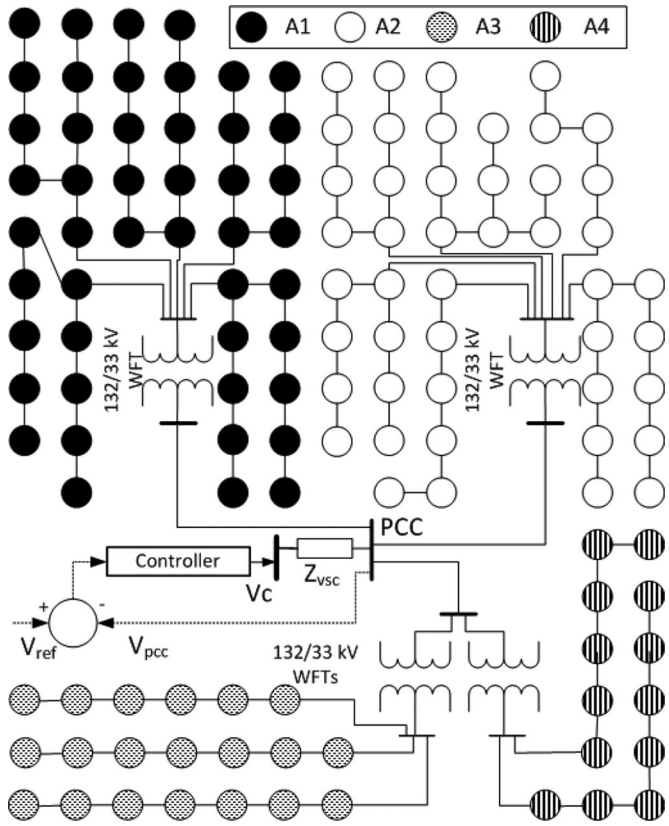

Fig. 1. Layout of the wind farm system.

II. Description of a Wind Farm

A model wind farm system shown in Fig. 1 comprises two wind farms, Wind Farm-1 (WF1) and Wind Farm-2 (WF2) with capacity 465 MW (93 × 5MW) and 165 MW (33 × 5 MW), respectively. It is divided into four areas, A1 to A4: A1 and A2 are part of WF1, whereas A3 and A4 are part of WF2.

The wind farms use PMSG type WTGs interconnected using a network of 33 kV collector cable strings. A circle in Fig. 1 represents a WTG and its WTG transformer. Four shades are used in the circles to distinguish WTGs of different areas. Five to ten WTGs are connected using 33 kV cable sections to form a string. Many strings are connected to low voltage side of 33/132 kV wind farm transformer (WFT). The distance of each 33 kV sections is assumed to be 1 km. Three 132 kV cables of 30 km length connect the WFTs to the point of common coupling (PCC) where the VSC of the HVDC line is located. All the cable parameters are available in [10]. For the purpose of this analysis, the HVDC system is represented using a VSC, which is modelled using a converter voltage behind an impedance and a controller which regulates the PCC voltage magnitude by controlling the converter voltage. The DC side of the HVDC line is not modelled as the main focus of this paper is on the analysis of wind farm collector system modes.

III. Modelling of Wind Farm

A detailed model of the wind farm system is developed using the Matlab/ Simulink platform. The PMSGs, transformers, cable sections, VSC, and VSC controller are represented in the program without resorting to aggregation techniques in order to preserve all oscillatory modes in the collector system.

A. Modelling of PMSG Based WTG

Fig. 2 shows PMSG configuration used in this study. A model of PMSG comprises of equations representing the back to back converter, generator, generator-turbine mechanical dynamics, turbine aerodynamics equation relating wind speed to mechanical torque, and blade pitch angle controller. The circles in Fig. 1 correspond to all components in Fig. 2 except the impedance between Bus 2 and Bus 3 which is used to form a single machine infinite bus (SMIB) test system. The WTG uses an LCL filter which is widely used in wind turbines to remove switching frequency components. The R-L-C parameters of WTG transformer and infinite bus impedance at 5 MVA base are 0.0077-0.0665-6.8e-5 (p.u.) and 0.015-0.15-0.010 (p.u.), respectively.

1) Representation of PMSG: The PMSG in d-q synchronous reference frame is represented using (1)–(5)

$$L_s^d p i_s^d = -e_s^d + L_s^q i_s^q \omega_r - R_s i_s^d \tag{1}$$

$$L_s^q p i_s^q = -e_s^q - L_s^d i_s^d \omega_r + \phi_{pm}\omega_r - R_s i_s^q \tag{2}$$

$$P_s = e_s^q i_s^q + e_s^d i_s^d \tag{3}$$

$$Q_s = e_s^q i_s^d - e_s^d i_s^q \tag{4}$$

$$T_e = i_s^q(\phi_{pm} + (L_s^q - L_s^d) i_s^d) \tag{5}$$

where $p = d/dt$. Parameters L_s, R_s, and ϕ_{pm} represent stator inductance, stator resistance and rotor flux of the generator, respectively. Variables e_s, i_s, ω_r, P_s, Q_s, and T_e are voltage, current, rotor speed, stator active power, stator reactive power and electrical torque produced in the air gap, respectively. Superscripts q and d indicates that the respective parameters refer to the quadrature and direct axes, respectively.

The output of the generator is fed to a back to back converter formed of a machine side converter (MSC) and a grid side converter (GSC). Together they convert a low frequency ac voltage to 50 Hz voltage. The dynamics (switching level) the converters are much faster than the electrical dynamics considered in this study. Hence for fundamental frequency modelling, simplified model (space vector dq model) of converter is considered such that the output voltage of converter is equal to target voltage demanded by converter controller. Dynamics of the converter capacitor voltage is expressed as,

$$C p v_{dc} = (P_s - P_i)/v_{dc} \tag{6}$$

where P_i is output of GSC, and v_{dc} is capacitor voltage.

It is reported in many literatures and also found in this study (Section V) that the back-to-back converter divides the system into two such that the oscillatory modes have participation only from the states located at one of the two sides [11]. For example, oscillatory modes with participation from states related to the collector system show no participation from states related to the generator or turbine, and vice versa. Hence, for the analysis of modes in the collector system, the explanation of generator, turbine and MSC controller models are not included. The MSC

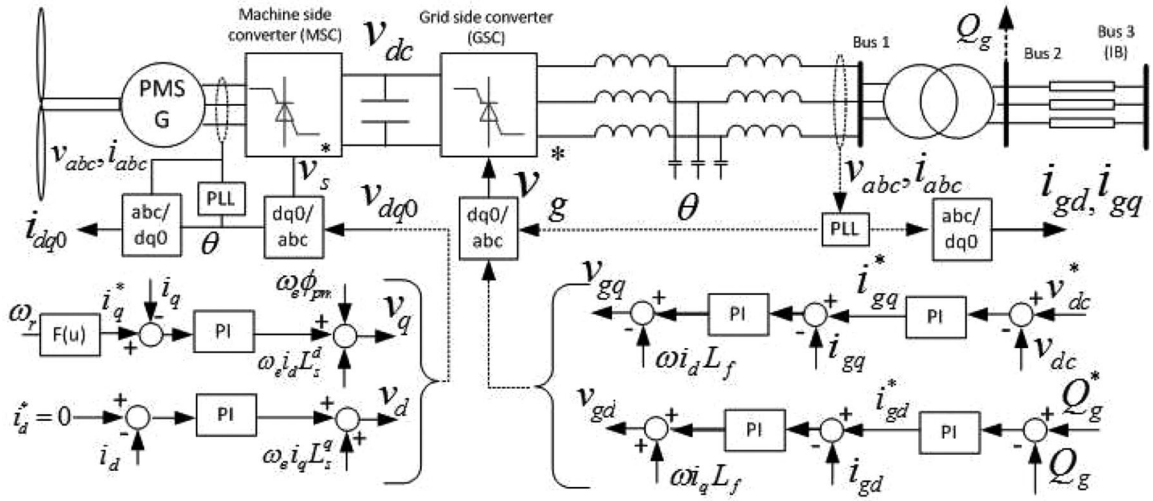

Fig. 2. PMSG SMIB system.

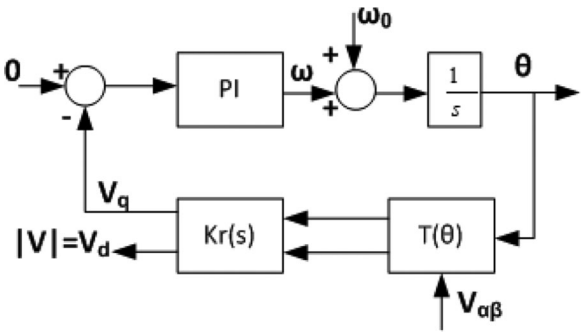

Fig. 3. Simplified block diagram of the PLL system.

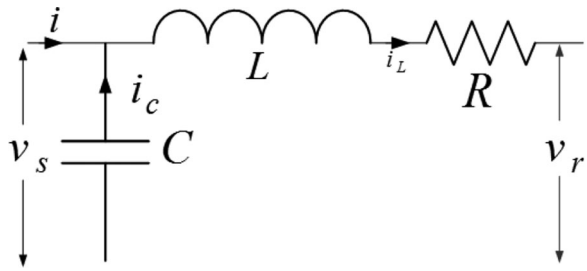

Fig. 4. Γ section representing cable, transformer and converter impedance.

controller as shown in Fig. 2 is similar to GSC controller, which is described in the next subsection. Moreover many literature [10], [11] describe the turbine and generator modelling in detail.

2) Representation of GSC: Neglecting fast converter dynamics the output of GSC controller (v_g^*) is assumed as the output of GSC ($v_g^* = v_i$). The GSC controller in Fig. 2 has two cascaded PI loops in q and d axis with feed forward term to improve transient response of the system. The outer q-axis PI controller regulates capacitor voltage such that active power produced by the PMSG is transferred to the grid. The outer d-axis PI controller regulates reactive power output of the WTG measured at the high voltage terminal of the WTG transformer to a predefined reference value. The inner PI controllers are fast current controllers which generate reference converter voltage. A phase locked loop produces the phase angle reference for the controller to keep it synchronised with the grid. A structure of the PLL [12] is shown in Fig. 3.

For clarity of presentation, the states inside the GSC controller are named as, gsc_x^y, where $x = p$ if the state is located in the active power or capacitor voltage control loop, $x = q$ if the state is located in the reactive power control loop, $y = in$ if it is in the inner PI controller, and $y = out$ if it is in the outer PI controller. The states associated with PLL are named as PLL_{int}, PLL_{pi}, and PLL_{rsvr} for states representing the integrator, the PI controller and the resolver, respectively.

3) Representation of LCL Filter: (7)–(9) represent the LCL filter in the D-Q reference frame where D-axis leads Q-axis.

$$\frac{L_i}{\omega_b} p i_i = v_i - v_{cf} - (R_i + R_{cf}) i_i + T\omega L_i i_i + R_{cf} i_g \quad (7)$$

$$\frac{L_g}{\omega_b} p i_g = v_{cf} - v_g - (R_g + R_{cf}) i_g + T\omega L_i i_g + R_{cf} i_i \quad (8)$$

$$\frac{C_f}{\omega_b} p v_{cf} = i_i - i_g - T\omega C_f v_{cf} \quad (9)$$

where $i_i = [i_i^Q, i_i^D]'$, $i_g = [i_g^Q, i_i^D]'$, $v_i = [v_i^Q, v_i^D]'$, $v_g = [v_g^Q, v_g^D]'$, and $v_{cf} = [v_{cf}^Q, v_{cf}^D]'$ are inverter side inductor current, grid side inductor current, inverter output voltage, filter output voltage, and filter capacitor voltage, respectively and matrix T is given by $T = [1, 0; 0, -1]$

B. Representation of Transformers and Cables

Components such as cables, transformers, WTG GSC side filter, and VSC converter impedance are distinctly different in terms of their construction, size and role. However, for the dynamic simulation of a balanced system, they are represented using a R-L-C Π section. When connected in series, it is equivalent to connecting several Γ sections as in Fig. 4. Differential

equations representing a Γ section are given in (10)-(11).

$$\frac{L}{\omega_b} p i_L = v_s - v_r - R i_L + T\omega L i_L \tag{10}$$

$$\frac{C}{\omega_b} p v_s = i - i_L - T\omega C v_s \tag{11}$$

The subscripts, s, and r stand for sending end, and receiving end, respectively, and the current and voltages are marked in the Fig. 4. Also $i_L = [i_L^Q, i_L^D]'$, $i = [i^Q, i^D]'$, $v_s = [v_s^Q, v_s^D]'$ and $v_r = [v_r^Q, v_r^D]'$.

C. Representation of VSC Controller

VSC transfers energy from the wind farm network to DC line, and controls voltage and frequency at the PCC [13]. For a fundamental frequency modelling such as this work, the only feedback loop required for the VSC is the voltage magnitude as the frequency and phase angle are predefined. The PCC voltage is compared with a reference voltage and fed to an VSC controller as shown in Fig. 1. Neglecting converter dynamics the output of the controller is assumed as the converter voltage.

IV. Design of LCL Filter, PLL and GSC Controller

This section explains design of LCL filter, PLL and GSC controller using the SMIB test system which have been used in the wind farm modelling. More than one designs are prepared for each of the components in order to study the sensitivity of design parameters on the oscillatory modes in the SMIB system and wind farm system.

A. Design of LCL Filter

An LCL filter which has small dependence on the grid parameters, better attenuation, and capability to limit inrush current is used to smoothen the output voltage. However it brings resonance problem that requires a passive damping resistance contributing to filter power losses. Many literature describes design of LCL filter and two designs (LCL-1 [14] and LCL-2 [15]) are presented in this paper for comparison. Both methods are similar but provides different parameters and are used to analyse the sensitivity of LCL design on the wind farm dynamics.

Let assume base MVA, base voltage, base frequency, converter capacitor, and converter switching frequency as S_b= 5 MVA, $V_b = 1$ kV, $\omega_b = 2\pi 50$, V_{dc}=4.8 kV, and $f_{sw} = 5$ kHz, respectively. Using these assumptions the base impedance, base inductance and base capacitance are calculated as $Z_b = 0.2\ \Omega$, L_b= 0.64 mH, and $C_b = 15900\ \mu$F, respectively.

1) LCL1: Inductance at the converter side, L_i and the grid side, L_g are selected as 5% (L_i=31.8 mH) and 0.15% (L_g=0.95 μH), respectively. Considering 6.65% transformer inductance, total inductance at grid side is 6.8%. Assuming 5% capacitance, corresponding resonance frequency is 1.317 kHz which is in the acceptable range, between ten times line frequency and one half of the switching frequency (assuming 5 kHz switching frequency). The damping resistance, R_{cf}, is calculated as one third of the impedance of capacitance at resonance frequency which is equal to 0.055 Ω.

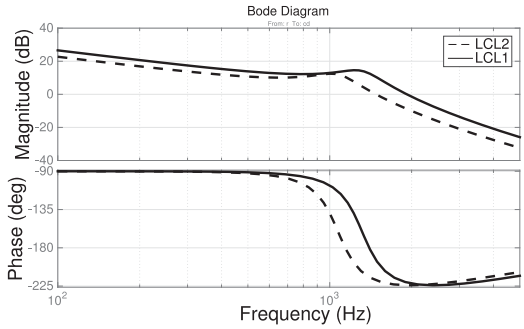

Fig. 5. LCL filter bode of transfer function i_g/v_i.

TABLE I
Parameters of different PLLs

Name	T_r (msec)	K_p	K_i	Bandwidth (Hz)
PLL-1	5	81	2722	21.8
PLL-2	10	40	680	10.9
PLL-3	20	20	170	5.4

2) LCL2: Assuming 20% ripple reduction in the inverter side inductor, $Li = 0.663 V_{dc} V_{ph}/(p_n f_{sw})$ is calculated as 11.5% (L_i=0.073 mH), where $P_n = 5$ MW. For 2% output current ripple, ratio between inductances is assumed as six that gives total output inductance $L_g + L_{tr}$=0.044 mH or 6.9%. Assuming 5% capacitance, corresponding resonance frequency is 1.075 kHz which is in the acceptable range. The damping resistance, R_{cf}, is calculated as 0.062 Ω. Fig. 5 shows bode diagram of the transfer function i_g/v_i for both the designs.

B. Phase Locked Loop

PLL is used to synchronise the WTG to grid through detection of positive sequence voltage phase at fundamental frequency [12], [16]. The PLL structure used for developing WTG model is shown in Fig. 3. It contains a resolver delay, $K_r = 1/(1 + sT_r)$, which depends on the method used to calculate q and d axis voltages from three phase voltages. The PLL locks by driving the q-axis term to zero using a PI controller. The output of the PI controller is a frequency term which is integrated to obtain phase angle.

One of the objectives of this paper is to discuss influence of PLL response in the wind farm oscillatory modes. Hence three designs of PLL are prepared for three different values of resolver delay, $T_r = 5$ msec, 10 msec, and 20 msec. For clarity of presentations the PLL designs are named as PLL-1, PLL-2, and PLL-3. Table I lists PI controller parameters and bandwidth obtained for each of the designs. The step response of the PLL is shown in Fig. 6 for comparison.

C. GSC Controller

The SMIB test system shown in Fig. 2 is used for the controller tuning. The GSC controller tuning involves finding parameters of four PI controllers. The cross coupling terms ($L_f i_d$ and $L_f i_q$) are assumed as exogenous input during this process, where

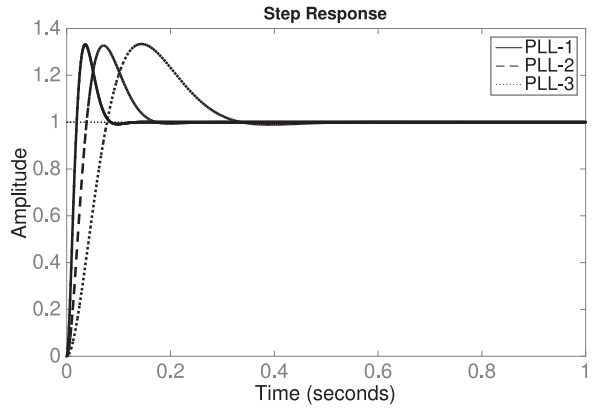

Fig. 6. Step response of different PLLs.

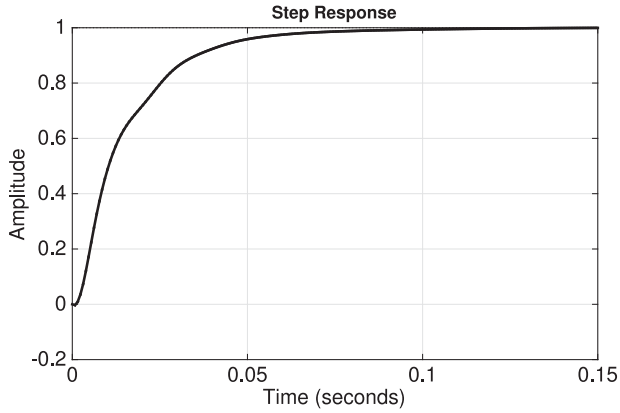

(a)

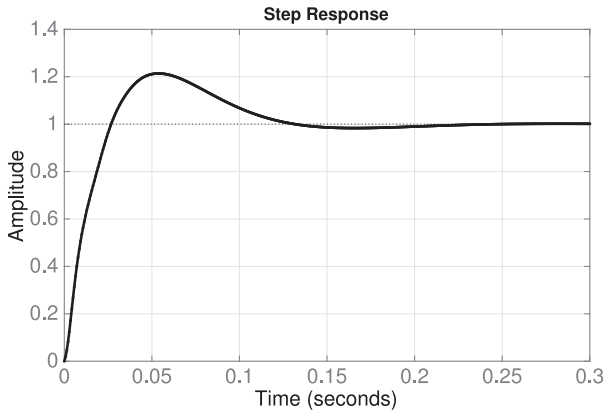

(b)

Fig. 7. Step response of GSC (a) reactive power and (b) capacitor voltage control loop.

$L_f = L_i + L_g$. The inner current control loop is tuned for a bandwidth of 100 Hz.

The outer loops are generally tuned one decade slower than inner loop. Fig. 7 shows step response of the controller for 10 Hz bandwidth. However, in order to study the sensitivity of the GSC controller parameters on the wind farm oscillatory modes, three designs, GSC-1, GSC-2, and GSC-3, are prepared considering the outer loop bandwidth 5 Hz, 10 Hz and 20 Hz, respectively. The LCL-1 parameters are used for these designs. Another GSC controller, GSC-4 is prepared with 10 Hz outer loop bandwidth for the system using LCL-2. The parameters of the GSC PI controllers are listed in Table II.

TABLE II
PMSG GSC CONTROLLER PARAMETERS

Case	Inner Loops		Outer Q loop		Outer $V_{dc}loop$	
	K_p	K_i	K_p	K_i	K_p	K_i
GSC-1	0.3	200	0	-31	-11.5	-268
GSC-2	0.3	200	0	-62	-22.5	-872
GSC-3	0.3	200	0	-116	-38.5	-3489
GSC-4	0.45	290	0	-61	-20	-977

D. Modal Analysis Tools

The wind farm model discussed in this paper is programmed using MATLAB/Simulink software. The linearised model of the system under a steady state operating condition is obtained using the command *linmod* [17], which returns state matrix **A**, input matrix **B**, output matrix **C**, and feedforward matrix **D** of the linearised system. The eigenvalues $\{\lambda_i = \sigma_i \pm j\omega_i\}_1^n$, right eigenvector $\boldsymbol{\phi_i}$, and left eigenvector $\boldsymbol{\psi_i}$ of **A**, are obtained using *eig* command in the Matlab. The frequency and % damping ratio of a mode (λ_i) are found using the relations, $f = \omega/2\pi$ and $\zeta = -100\sigma/\sqrt{\sigma^2 + \omega^2}$, respectively. The relative participation of *k*th state variable in *i*th mode pf_{ki} is given as $pf_{ki} = (|\phi_{ik}||\psi_{ki}|)/(\sum_{k=1}^{k=n} |\phi_{ik}||\psi_{ki}|)$. While presenting the results in the following sections, normalised participation factor ($NPF = pf_{ki} \max(pf_{ki})$) is used.

V. ANALYSIS OF THE SMIB SYSTEM

This section discusses the characteristics of oscillatory modes in the SMIB system shown in Fig. 2, and the sensitivity of the modes to selected LCL filters, PLLs and GSC controllers. Apart from the GSC, PLL and LCL states, the SMIB system contains the following states: WTG transformer current states (i_{tr}^D and i_{tr}^Q), Bus-2 voltages states (v_{b2}^D and v_{b2}^Q), and transmission line current states ((i_{tl}^D and i_{tl}^Q). A superscript 'm' is used with the states of PLL at the MSC to differentiate it from the states of PLL at the GSC.

Eleven pairs of complex eigenvalues are observed in the SMIB test system. Two of them have frequency in the range of MHz due to 1 nF stray capacitance assumed for the WTG transformer, and another two have frequency 3.4 kHz with participation from the WTG transformer and transmission line states. All the four modes are insensitive to WTG parameter variation.

The frequency and damping ratio of the rest of the seven modes are listed in Table III for different combinations of LCL, PLL and GSC controller parameters. The cases in Columns 2, 5, and 8 are the same. The modes are classified based on the states participating in the modes and their NPF. The states participating in the mode along with corresponding NPF (in bracket) for the combination LCL-1, PLL-2, GSC-2 are listed in the Table IV.

The modes E1 and E2 are collector system modes having frequency around 1 kHz. They have participation from the states of the transformer, the transmission line and the LCL filter. The

TABLE III
CRITICAL OSCILLATORY MODES OF THE SMIB TEST SYSTEM FOR DIFFERENT COMBINATION OF LCL, PLL AND GSC CONTROLLER PARAMETERS

	LCL-1 PLL-2, GSC-2	LCL-2 PLL-2, GSC-4	GSC-1 PLL-2, LCL-1	GSC-2 PLL-2, LCL-1	GSC-3 PLL-2, LCL-1	PLL-1 LCL-1, GSC-2	PLL-2 LCL-1, GSC-2	PLL-3 LCL-1, GSC-2
Modes	Frequency - Hz (Damping Ratio - %)							
E1	1126 (11)	859 (8)	1126 (11)	1126 (11)	1126 (11)	1126 (11)	1126 (11)	1126 (11)
E2	1019 (12)	744 (9)	1019 (12)	1019 (12)	1019 (12)	1019 (12)	1019 (12)	1019 (12)
E3	95 (34)	95 (39)	94 (36)	95 (34)	97 (31)	95 (34)	95 (34)	95 (34)
E4	56 (29)	63 (36)	54 (34)	56 (29)	58 (21)	53 (29)	56 (29)	56 (29)
E5	5.1 (53)	5.4 (50)	3.3 (48)	5.1 (53)	11.3 (56)	5.8 (54)	5.1 (53)	5.5 (61)
E6	5.4 (77)	5.9 (72)	5.2 (74)	5.4 (77)	4.8 (70)	10.2 (78)	5.4 (77)	2.3 (68)
E7	93 (36)	93 (36)	93 (36)	93 (36)	93 (36)	191 (21)	93 (36)	39 (64)

The frequency in Hz and damping ratio in % (in bracket) are listed.

TABLE IV
PARTICIPATING STATES AND CORRESPONDING NPF OF THE SMIB SYSTEM MODES

Modes	States and corresponding NPF in bracket
E1	v_{cf}^D (1.0), v_{cf}^D (0.98), i_i^Q (0.86), i_i^D (0.84), i_{tl}^Q (0.17), and i_{tl}^D (0.17)
E2	v_{cf}^D (1.0), v_{cf}^D (0.98), i_i^D (0.85), i_i^Q (0.84), i_{tl}^D (0.16), i_{tl}^Q (0.15)
E3	gsc_p^{in} (1.0), i_{tl}^Q (0.95), i_{tl}^D (0.92),gsc_q^{in} (0.85) i_{tr}^Q (0.42), i_{tr}^D (0.39), i_i^Q (0.31), i_i^D (0.29)
E4	gsc_q^{in} (1.0), gsc_p^{in} (0.93), i_{tl}^D (0.38), i_{tl}^Q (0.28), gsc_q^{out} (0.18), i_{tr}^D (0.15), i_{tr}^Q (0.12), v_{dc} (0.13), i_i^D (0.1)
E5	PLL_{int} (1.0), gsc_p^{out} (0.75), v_{dc} (0.72), PLL_{rsvr} (0.44), PLL_{pi} (0.38), gsc_q^{out} (0.19)
E6	PLL_{int} (1.0), PLL_{rsvr} (0.8), PLL_{pi} (0.38), gsc_p^{out} (0.25), v_{dc} (0.22), gsc_q^{out} (0.17)
E7	PLL_{int}^m (0.95), i_s^d (0.43), i_s^q (0.2), PLL_{rsvr}^m(1.0)

modes E3 and E4 have participation from the states of the GSC controller and the participating states are located mostly in the GSC controller alone.

For E5 in the LCL-1, PLL-2, GSC-2 case the state PLL_{int} has highest participation and NPF from the GSC states gsc_p^{out} and v_{dc} follows. But for all the other cases, the NPF of the mode E5 from GSC states are higher. The mode E8 have higher participation from states of PLL and it is consistent for all the selected cases.

The mode E7 has participation from the states of PLL at MSC, and PMSG stator currents. The damping and frequency of the mode is affected by choice of PLL at MSC, and not by changes in the parameters at grid side of the converter. The damping of the mode is sufficient for stable operation under all the selected cases. Another important observation is that, none of the oscillatory modes has participation from states located at both sides of the back-to-back converter, meaning the back-to-back converter effectively blocks the oscillations from one side to another. Hence, for further discussions in this paper, the modes located at machine side of the converter are not considered.

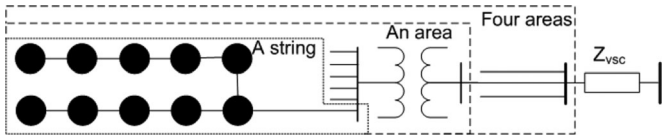

Fig. 8. Representation of a string, an area, four areas connected to the PCC and four areas connected to infinite bus through VSC impedance.

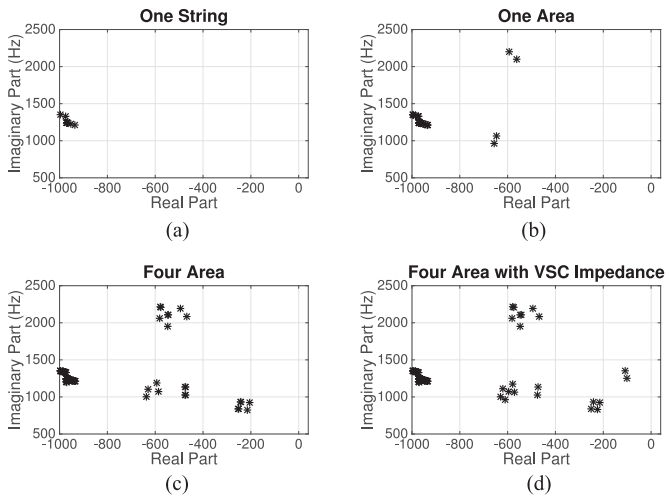

Fig. 9. Subsystems's oscillatory modes in the 500 Hz to 2.5 kHz range.

Comparing frequency and damping ratio of the modes for all the selected cases, the system is found to be very stable. In the remaining part of this paper, the WTG using these parameters is used in a full wind farm system to analyse resulting oscillatory modes in it. However, before considering the full wind farm system, the following section presents evolution of critical modes with accumulation of many PMSGs and collector strings.

VI. EVOLUTION OF MODES WITH SYSTEM COMPLEXITY

Analysis of four wind farm subsystems such as a string, an area, four areas and the full wind farm system without VSC controller, are discussed in this section. The boundary of the subsystems are marked in Fig. 8. The subsystem modes have frequency ranging from Hz to several MHz. Very high frequency modes are excluded from the discussion. Figs. 9, 10, 11, and 12

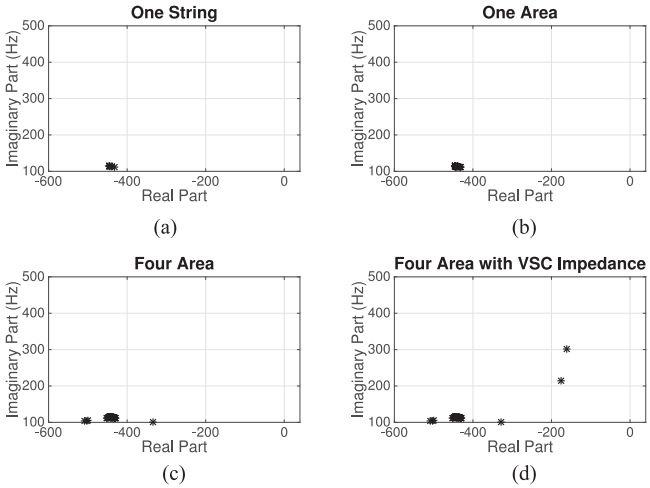

Fig. 10. Subsystems's oscillatory modes in the 100 Hz to 500 Hz range.

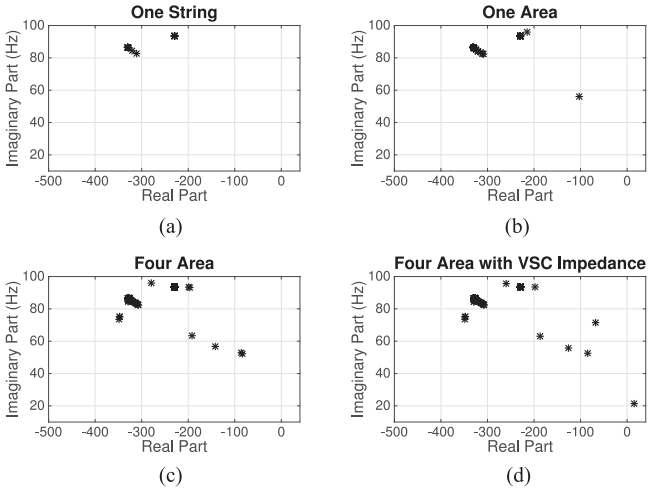

Fig. 11. Subsystems's oscillatory modes in the 10 Hz to 100 Hz range.

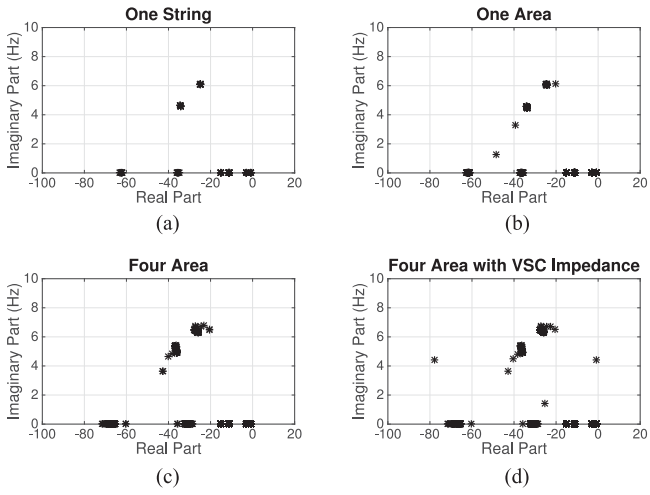

Fig. 12. Subsystems's oscillatory modes in the 1 Hz to 10 Hz range.

show modes of the four subsystems in four different frequency ranges: 500 to 2500 Hz, 100 to 500 Hz, 10 to 100 Hz, and 1 to 10 Hz, respectively. Each figure has four sub figures corresponding to four sub systems.

The string subsystem contains ten WTGs and nine cable sections. All modes of the string subsystem are stable. The area subsystem contains 47 WTGs, a WFT and many 33 kV collector cable strings. The majority of the area subsystem modes are close to the string subsystem modes. However, couple of modes in each of the frequency ranges are shifted. This is due to the higher impedance of the WFT. Similarly, for the remaining two subsystems the few modes are distinct.

As many WTGs and collector strings are accumulated, some of the modes shifts towards poor damping region. One such case is where the two modes with frequency close to 300 Hz and 200 Hz in the Fig. 10(d). They are named M1 and M2, respectively. These modes were part of the above 500 Hz frequency range, and shifted down due to the higher impedance of the VSC. Characteristics of these modes are discussed in the Section VII.

Similarly, a mode, named M3, with negative damping appears near 20 Hz region in Fig. 11(a) and another one, named M4, with poor damping appears near 5 Hz region in Fig. 12(d). The sub figures in each frequency range tracks the evolution of modes as the WTGs and cables are accumulated. The next section describes characteristics and sensitivity of the critical modes (M1-M4) in detail.

VII. Characteristics of Critical Modes

This section will focus on the full wind farm system as shown in Fig. 1 but without including the VSC controller. Such a system without the controller will not exist in practice but will help in this study to characterise the critical modes before designing the controller and get insight of the sensitivity of the modes to PMSG parameters. Four critical modes listed in Table V are selected for detailed analysis .

A. Participation Factor Analysis

The discussions on participation factor analysis use the results obtained using LCL-1, PLL-2 and GSC-2 combination in the PMSG . Frequencies of two of the modes, M1 (301.6 Hz) and M2 (214.1 Hz) are close to the harmonics of the power frequency. The states participating in these modes and corresponding NPF are listed in Tables VI and VII, respectively, and it is evident that all the states participating in these modes are related to collector system components of the wind farm. No significant participation is observed from the PMSG states and their damping ratios are sufficient considering the frequencies for stable operation.

Table VIII lists the states and NPF of the mode M3 which has frequency 21.4 Hz and damping ratio -11.5%. Large share of participation of M3 is taken by two states i_{vsc}^{D} and i_{vsc}^{Q} which are related to VSC impedance. The other states, from collector system and PMSG GSC controller, gets significantly lower proportion of NPF. Participation from gsc_{p}^{in}, $v_{d}c$, gsc_{q}^{in}, and gsc_{q}^{out} of all the PMSGs in the wind farm is observed. However, what is

TABLE V
FREQUENCY AND DAMPING RATIO OF THE CRITICAL MODES IN THE WIND FARM SYSTEM WITHOUT VSC CONTROLLER

	LCL-1 PLL-2, GSC-2	LCL-2 PLL-2, GSC-4	GSC-1 PLL-2, LCL-1	GSC-2 PLL-2, LCL-1	GSC-3 PLL-2, LCL-1	PLL-1 LCL-1, GSC-2	PLL-2 LCL-1, GSC-2	PLL-3 LCL-1, GSC-2
Modes				Frequency (Hz)				
M1	301.6	276.3	301.6	301.6	301.6	301.6	301.6	301.6
M2	214.1	195.9	214.1	214.1	214.1	214.1	214.1	214.1
M3	21.4	25.9	18.6	21.4	25.3	18.5	21.4	22.5
M4	4.3	4.3	2.8	4.3	6.3	5.4	4.3	5.6
				Damping Ratio (%)				
M1	8.4	9.6	8.4	8.4	8.4	8.4	8.4	8.4
M2	12.9	16.2	12.9	12.9	12.9	12.9	12.9	12.9
M3	−11.5	−4.7	−1.4	−11.5	−18.8	−23.1	−11.5	−11.1
M4	3.0	0.4	11.3	3.0	1.7	25.6	3.0	3.1

TABLE VI
STATES AND NPF OF MODE M1

State	NPF	State	NPF	State	NPF
v_{pcc}^{D}	1.00	v_{hvc1}^{D}	0.30	i_{A1wft}^{Q}	0.25
v_{pcc}^{Q}	0.99	v_{hvc2}^{D}	0.30	i_{A2wft}^{Q}	0.25
i_{vsc}^{Q}	0.57	v_{hvc1}^{Q}	0.30	i_{A3wft}^{Q}	0.10
i_{vsc}^{D}	0.57	v_{hvc2}^{Q}	0.30	i_{A3wft}^{D}	0.10
v_{hvc3}^{Q}	0.31	i_{A1wft}^{D}	0.25	i_{A4wft}^{D}	0.06
v_{hvc3}^{D}	0.31	i_{A2wft}^{D}	0.25	i_{A4wft}^{Q}	0.06

TABLE VII
STATES AND NPF OF MODE M2

State	NPF	State	NPF	State	NPF
v_{pcc}^{Q}	1.00	v_{hvc1}^{Q}	0.30	i_{A1wft}^{D}	0.28
v_{pcc}^{D}	0.99	v_{hvc2}^{Q}	0.30	i_{A2wft}^{D}	0.28
i_{vsc}^{Q}	0.52	v_{hvc1}^{D}	0.30	i_{A3wft}^{Q}	0.12
i_{vsc}^{D}	0.51	v_{hvc2}^{D}	0.30	i_{A3wft}^{D}	0.12
v_{hvc3}^{D}	0.31	i_{A1wft}^{Q}	0.29	i_{A4wft}^{D}	0.07
v_{hvc3}^{Q}	0.31	i_{A2wft}^{Q}	0.29	i_{A4wft}^{Q}	0.07

TABLE VIII
STATES AND NPF OF MODE M3

State	NPF	State	NPF
i_{vsc}^{D}	1.00	v_{hvc3}^{D}	0.034
i_{vsc}^{Q}	0.70	i_{A2wft}^{Q}	0.033
v_{pcc}^{Q}	0.114	gsc_{p}^{in} All PMSGs	0.019–0.023
v_{pcc}^{D}	0.098	i_{hvc1}^{D}	0.014
i_{A1wft}^{D}	0.049	i_{hv21}^{D}	0.014
i_{A2wft}^{D}	0.047	i_{A3wft}^{D}	0.014
v_{hvc1}^{Q}	0.041	v_{dc} All PMSGs	0.010–0.011
v_{hvc2}^{Q}	0.041	gsc_{q}^{in} All PMSGs	0.011–0.014
v_{hvc3}^{Q}	0.04	gsc_{q}^{out} All PMSGs	0.010–0.012
i_{A1wft}^{Q}	0.035	i_{hvc1}^{Q}	0.01
v_{hvc1}^{D}	0.035	i_{hv21}^{Q}	0.01
v_{hvc2}^{D}	0.035		

TABLE IX
STATES AND NPF OF MODE M4

State	NPF	State	NPF
i_{vsc}^{D}	1.00	v_{hvc3}^{Q}	0.02
i_{vsc}^{Q}	0.748	v_{hvc1}^{Q}	0.019
PLL_{int} All PMSGs	0.093–0.130	v_{hvc2}^{Q}	0.019
GSC_{q}^{out} All PMSGs	0.067–0.084	i_{A3wft}^{Q}	0.015
i_{A1wft}^{D}	0.063	i_{hvc1}^{D}	0.015
i_{A2wft}^{D}	0.062	i_{hvc2}^{D}	0.015
v_{pcc}^{Q}	0.059	i_{hvc1}^{Q}	0.013
v_{dc} All PMSGs	0.059–0.100	i_{hvc2}^{Q}	0.013
i_{A1wft}^{Q}	0.054	v_{hvc1}^{D}	0.013
i_{A2wft}^{Q}	0.054	v_{hvc2}^{D}	0.013
GSC_{p}^{out} All PMSGs	0.049–0.082	v_{hvc3}^{D}	0.012
PLL_{pi} All PMSGs	0.049–0.068	i_{A4wft}^{D}	0.011
v_{pcc}^{D}	0.033	GSC_{p}^{in}	0.011–0.014
PLL_{rslv} All PMSGs	0.025–0.034	GSC_{q}^{in}	0.010–0.012
i_{A3wft}^{D}	0.023	i_{hvc3}^{D}	0.01

interesting to note is that when the states related to PMSG have participation, though it is in smaller proportion, states from all the PMSGs are involved. This points towards a collective effort which suggests that PMSG controller parameters may influence the characteristics of the mode M3. Sensitivity analysis presented in the next section will provide more insight. This mode can be related to the modes E3 and E4 of the SMIB system considering their participating states.

The mode M4 has frequency 4.3 Hz and damping ratio 3.0%. Table IX lists states and NPF of the mode that have significant higher participation from two states related to VSC impedance and lower proportion of participation from some states in the collector system, PMSG GSC controller states and PMSG PLL states. Participation from PLL_{int}, GSC_{q}^{out}, v_{dc}, GSC_{p}^{out}, PLL_{pi}, and PLL_{rslv} related to all the PMSGs in the wind farm is observed. The mode can be related to E5 and E6 of the SMIB system which have similar participating states.

B. Sensitivity Analysis of the Critical Modes

Table V lists the frequency and damping ratio of the critical oscillatory modes in the wind farm system without VSC

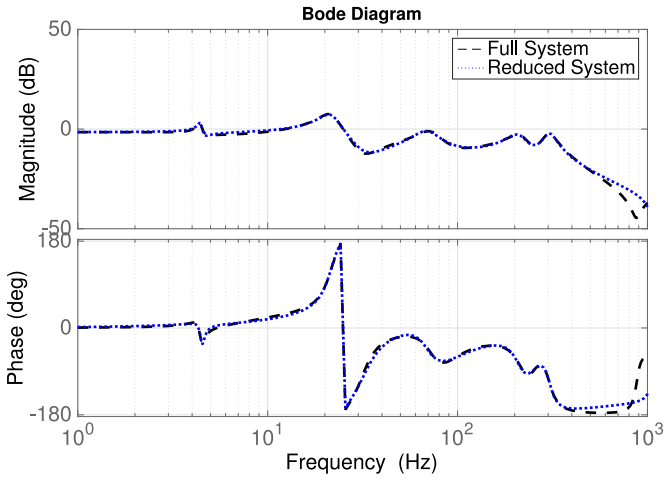

Fig. 13. Bode diagram comparing transfer function of the full wind farm system and 12th order reduced system.

controller. The colums (2-3) of the table show the effect of filter parameters, LCL-1 and LCL-2. The GSC controllers, GSC-1 and GSC-4, are tuned to obtained similar frequency response in the SMIB system using the LCL parameters, LCL-1 and LCL-2, respectively. All the four modes are sensitive to the changes in the filter parameters. The effect on the modes M1 and M2 can be attributed to their dependence on the collector system impedance that is changed in this case. The modes M3 and M4 have state participation from LCL and GSC controller states, and hence they are sensitive to the filter parameter changes.

The columns (4-6) of Table V list frequency and damping ratio of the critical modes for different GSC controller parameters. Same LCL and PLL parameters are used for the three cases. As discussed in the Section VII-A the modes M1 and M2 have participation only from states of collector system and hence no noticeable variation in the frequency and damping ratio are observed when different GSC controllers are used. However, significant changes are observed in the characteristics of the modes M3 and M4. This is inline with the observations made from the participation factor analysis where these modes show participation from the GSC states of all the WTGs.

The columns (7-9) of Table V list frequency and damping ratio of the critical modes for the different PLL designs. No changes are observed in the modes M1 and M2. However, Modes M3 and M4 show significant variation as they have participation from PLL states of the WTGs.

VIII. Mode Stabilization Using VSC Controller

A VSC controller is designed for the wind farm system using LCL-1, GSC-2, PLL-2 combination of parameters. In order to design the controller, a transfer function of the system is obtained considering the converter voltage as input and the PCC voltage as output. No zeros with positive real part is present in the transfer function. For controller design, the system transfer function is reduced to the order of 12. Fig. 13 shows bode plot of the full wind farm system and reduced order system. Both the plots show a close match in the frequency of interest. A PI

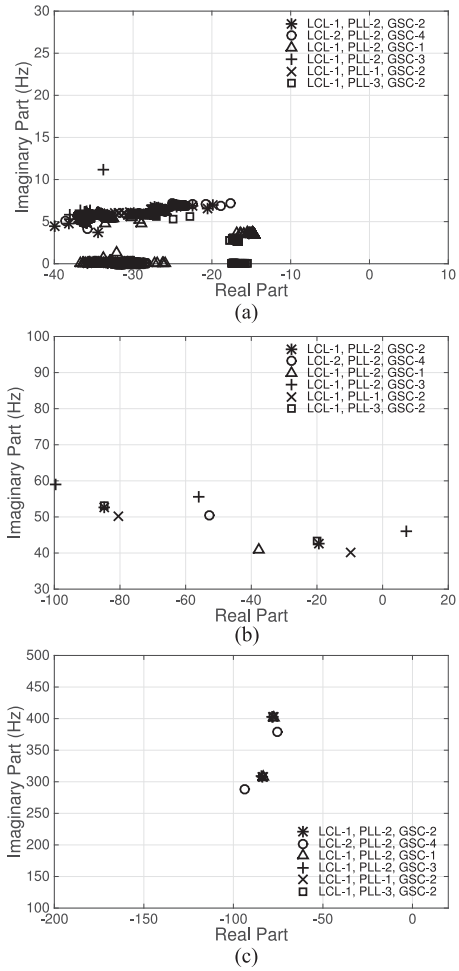

Fig. 14. Closed loop eigenvalues using different LCL filters, GSC controllers, and PLLs.

controller with $K_P = 3.5$ and $K_I = 800$ is found to stabilize the system for the selected wind farm configuration.

The close loop eigenvalues of the wind farm system with the different LCL filter, GSC controller and PLL combinations are plotted in Fig. 14. Similar to the variation in damping ratio observed in the sensitivity analysis of the wind farm system without the controller, the damping ratio of the modes in the closed loop system show large variation. For the range in frequency shown in Fig. 14(a) and (b) all the modes are stable for the selected cases. However, there appears a mode in 40 Hz to 60 Hz frequency range, which is related to the mode M3, whose damping varies considerably for different combinations of parameters. For example in the case of LCL-1, PLL-2, GSC-3 combination the closed loop system is unstable and in the case of LCL-1, PLL-1, GSC-3 combination it is poorly stable.

The dynamic simulation results shown in Fig. 15(a), (b), and (c) establishes the effect of different GSC controllers on the operation of wind farm system. The critical mode close to 40 Hz sets up an oscillation in the collector system which affects response of the system. For the set of parameters GSC-3, PLL-2, LCL-1, the system is unstable. The results shows that PMSG parameters have significant influence on the design of VSC

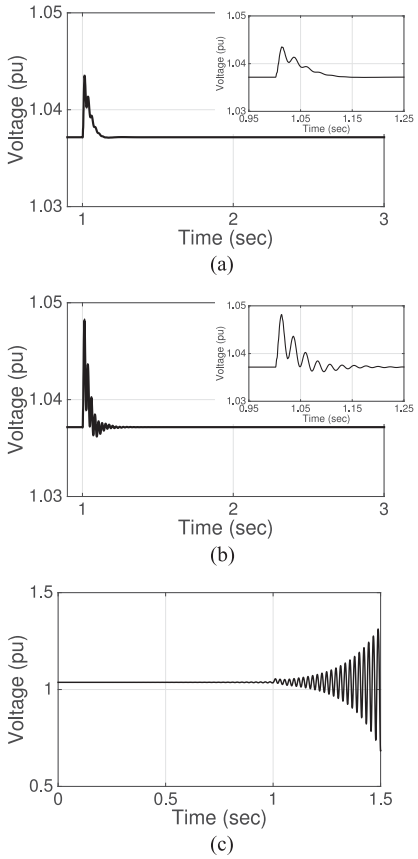

Fig. 15. PCC voltage following a step change in reactive power reference of all WTGs for the case (a) GSC-1, PLL-2, LCL-1 (b) GSC-2, PLL-2, LCL-1, and (c) GSC-3, PLL-2, LCL-1.

controller requiring a robust tuning considering individual wind farm configuration and WTG characteristics. A slower GSC controller improved the stability of the system. However, GSC settings are influence by fast reactive power/ voltage control response demanded in grid codes. A coordinated tuning of various controllers in wind farm is essential.

IX. Comparison Between Full and Aggregated Model

The critical oscillatory modes of the wind farm system with VSC-HVDC control are discussed in the previous section. It is clear that the characteristics of the modes depend on many wind farm parameters. In the power system studies it is imperative to represent a wind farm using an aggregated model that preserve the characteristics of the critical modes, and the influence on their characteristics by the wind farm parameters. In this section, a comparison is presented between the full wind farm system modes and an aggregated wind farm system modes to show that how a simple aggregation [18] can result in misleading conclusions.

An aggregated model of the wind farm is developed such that three aggregated WTGs represent generation from WF1 A1, WF1 A2, and WF2. In each of the three parts of the wind farm, the WTGs, the WTG transformers, and the 33 kV cable and the WFT are aggregated, and represented using an equivalent machine, a transformer, and an impedance, respectively. The capacity of the aggregated WTGs are equal to total installed capacity of the aggregated area or wind farm. The parameters of the machine, filter and WTG transformer of the aggregated machine at the aggregated machine base are equal to the corresponding parameters at individual machine base (5 MW). The 33 kV collector strings and WFT are represented using an aggregated impedance such that apparent power loss in the aggregated impedance is equal to the apparent power loss in the 33 kV section and the WFT. The representation of the three 132 kV cables, and the VSC impedance and control are unchanged. Similarly, the control parameters at PMSG and VSC-HVDC are not altered.

TABLE X
Modes of the Full Wind farm System and the Aggregated Wind Farm System

Modes with $0.1 < f < 500$ Hz, and $\zeta < 40\%$					
Full wind farm system			Aggregated wind farm system		
Modes	f (Hz)	ζ (%)	Modes	f (Hz)	ζ (%)
F1	402	3.1	A1	345	−0.8
F2	308	4.3	A2	251	−1.4
F3	86	24.4	A3	115	29.5
F4	93	31.9	A4	113	29.6
F5	56	34.5	A5	103	19.4
F6	53	24.9	A6	33	5.9
F7	43	7.2	A7	36	9.5
			A8	35	7.1

Table X shows the modes of the full wind farm system and the aggregated wind farm system in the frequency range 0.1 Hz to 500 Hz and damping ratio less than 40%. First of all, there are differences in the number of modes, and their frequency and damping. In the selected frequency band, full wind farm system has seven modes and all are stable where as the aggregated wind farm system has eight modes and two of them are unstable. Setting aside the difference in frequency and damping ratio, it is found that the modes F1 and F2, and A1 and A2, respectively, have similar states participating on them, however, with difference in NPF. The F3 to F7 have majority participation from VSC, WFT, HV cable states and minority participation from the states of all the PMSGs. However, modes in the similar frequency range in the aggregated system such as A3 to A8 has higher participation from the aggregated PMSG states and lower participation from the VSC states. This will have impact on any controller designed using one model on the another. Also the frequency and damping of the respective modes are different in the two systems. Researchers must address this problem and find suitable methods such that both the full wind farm system and the aggregated system produce same response to a power system event.

X. Conclusion

This paper discusses oscillatory modes present in an offshore wind farm system connected to a VSC-HVDC system using modal analysis tools. There are multiple oscillatory modes in the system with poor damping ratio. Using participation factor analysis it is shown that the characteristics of the modes are

influenced by the PMSG parameters, such as GSC controller, PLLs, LCL filter, and controller parameters of VSC-HVDC. Both frequency and damping of the collector system modes changes with changes in the parameters. Comparison of a full system model and an aggregated system model shows significant differences in their dynamic characteristics. The results show that a simple aggregation of the wind farm system can result in misleading conclusions in power system analysis.

ACKNOWLEDGMENT

The authors would like to thank the late Dr. C. Oates of GE Grid Solutions (formerly Alstom Grid UK) for his valuable guidance and technical support for this work. Data supporting this publication can be obtained on request from cap-publications@imperial.ac.uk.

REFERENCES

[1] A. Woyte, J. D. Decker, and V. V. Thong. "A north sea electricity grid [r]evolution: Electricity Output of Interconnected Offshore Wind Power. A Vision of Offshore Wind Power Integration," Greenpeace Belgium, Brussels, Belgium, Sep. 2008. [Online] http://www.greenpeace.org/eu-unit/Global/eu-unit/reports-briefings/2009/5/A-North-Sea-electricity-grid-(r)evolution.pdf

[2] I. Erlich *et al.*, "Overvoltage phenomena in offshore wind farms following blocking of the HVDC converter," in *Proc. IEEE Power Energy Soc. General Meeting*, 2016, pp. 1–5.

[3] M. Bradt *et al.*, "Harmonics and resonance issues in wind power plants," in *Proc. 2011 IEEE Power Energy Soc. General Meeting*, San Diego, CA, 2011, pp. 1–8.

[4] M. Cheah-Mane, L. Sainz, J. Liang, Jun, and N. Jenkins, "Electrical resonance instability study in HVDC-connected offshore wind power plants," in *Proc. IEEE Power Energy Soc. General Meeting*, 2016, pp. 1–5.

[5] L. Wang and M. S. N. Thi, "Stability analysis of four PMSG-Based offshore wind farms fed to an SG-based power system through an LCC-HVDC link," *IEEE Trans. Ind. Electron.*, vol. 60, no. 6, pp. 2392–2400, Jun. 2013.

[6] H. Liu and J. Sun, "Voltage stability and control of offshore wind farms with AC collection and HVDC transmission," in *IEEE J. Emerg. Sel. Topics Power Electron.*, vol. 2, no. 4, pp. 1181–1189, Dec. 2014.

[7] D. Huang and Y. Mao, "The study of control strategy for VSC-HVDC applied in offshore wind farm and grid connection," in *Proc. Asia-Pacific Power Energy Eng. Conf.* Wuhan, 2011, pp. 1–4.

[8] M. Amin, M. Molinas, and J. Lyu, "Oscillatory phenomena between wind farms and HVDC systems: The impact of control," in *Proc. IEEE 16th Workshop Control Model. Power Electron.*, Vancouver, BC, 2015, pp. 1–8.

[9] R. Dimitrovski and M. Luther, "Investigation of harmonic Interaction between VSC-HVDC systems and offshore wind farms with DFIGs," in *Proc. IEEE Power Energy Soc. General Meeting*, 2016, pp. 1–5.

[10] L. P. Kunjumuhammed, B. C. Pal, C. Oates, and K. J. Dyke, "Electrical oscillations in wind farm Systems: Analysis and insight based on detailed modeling," *IEEE Trans. Sustainable Energy*, vol. 7, no. 1, pp. 51–62, Jan. 2016.

[11] H. Huang, C. Mao, J. Lu, and D. Wang, "Small-signal modelling and analysis of wind turbine with direct drive permanent magnet synchronous generator connected to power grid," in *IET Renew. Power Generation*, vol. 6, no. 1, pp. 48–58, Jan. 2012.

[12] S.-K. Chung, "A phase tracking system for three phase utility interface inverters," *IEEE Trans. Power Electron.*, vol. 15, no. 3, pp. 431–438, May 2000.

[13] L. Xu, L. Yao, and C. Sasse, "Grid integration of large DFIG-based wind farms using VSC transmission," *IEEE Trans. Power Syst.*, vol. 22, no. 3, pp. 976–984, Aug. 2007.

[14] M. Rosyadi, S. M. Muyeen, R. Takahashi, and J. Tamura, "New controller design for PMSG based wind generator with LCL-filter considered," in *Proc. XXth Int. Conf. Elect. Mach.*, Marseille, 2012, pp. 2112–2118.

[15] S. V. Araujo, A. Engler, B. Sahan, and F. L. M. Antunes, "LCL filter design for grid-connected NPC inverters in offshore wind turbines," in *Proc. 7th Int. Conf. Power Electron.*, Daegu, 2007, pp. 1133–1138.

[16] R. Teodorescu, M. Liserre, and P. Rodriguez, *Grid Converters for Photovoltaic and Wind Power Systems*. New York, NY, USA: Wiley, 2011

[17] *Online Technical Documentation of MATLAB*, The MathWorks Inc., Natick, MA, USA, 2015. [Online]. Available: http://www.mathworks.co.uk/help/techdoc/

[18] E. Muljadi, S. Pasupulati, A. Ellis, and D. Kosterov, "Method of equivalencing for a large wind power plant with multiple turbine representation," in *Proc. Power Energy Soc. General Meeting—Convers. Delivery Elect. Energy 21st Century*, Pittsburgh, PA, 2008, pp. 1–9.

Linash P. Kunjumuhammed (S'01–M'13–SM'16) received the B.Tech. degree from Mahatma Gandhi University, Kottayam, India, the M.S. degree from the Indian Institute of Technology Madras, Chennai, India, and the Ph.D. degree from Imperial College London, London, U.K., in 2002, 2006, and 2012, respectively, all in electrical engineering.

He was a Graduate Apprentice Trainee with Neyveli Lignite Corporation Ltd., Neyveli, India, from September 2002 to August 2003. In 2006, he joined the Advanced Engineering Group, TVS Motor Company Ltd. Hosur, India, and in 2008, he joined Imperial College London as a Research Assistant. From September 2012 to February 2013, he was with GE Global Research-Europe, Munich, Germany, as a Marie Curie Research Fellow, Secondment from Imperial College London, under the REAL-SMART project funded by the Marie Curie FP7 IAPP scheme. Since 2013, he has been working as a Research Associate at Imperial College London. His research interests include power system dynamics stability and control, renewable electricity generation, and wind farm dynamics.

Bikash C. Pal (M'00–SM'02–F'13) is a Professor of power systems at Imperial College London, London, U.K. His research interests include power system stability, control, and computation. He has graduated 17 Ph.D.s and published 70 technical papers in IEEE Transactions and IET journals. He has coauthored two books and two award winning IEEE Task Force/Working Group reports. He is the Editor-in-Chief of the IEEE TRANSACTIONS ON SUSTAINABLE ENERGY and a Fellow of IEEE for his contribution to power system stability and control.

Robin Gupta received the M.Tech. degree in electrical engineering from IIT Kanpur, Kanpur, India, in 2008. He is a Lead Researcher with GE HVDC R&D, U.K. His research interests include modelling, simulation, and control system design for power electronics converters. He has more than eight years of experience working for corporate research.

Kevin J. Dyke (M'05–SM'16) received the M.Eng degree in electrical and electronic engineering from the University of Manchester Institute of Science and Technology, Manchester, U.K., in 2005, the Postgraduate Diploma in management science from Manchester Business School, Manchester, U.K., in 2007, and the Eng.D. degree from the University of Manchester, Manchester, U.K., in 2009. He is currently the HVDC Research and Technology Manager at Alstom Grid Stafford. He is a Chartered Engineer with the IET, and member of the ILM and STEMnet.